

PAPER

Recovery from mechanical degradation of graphene by defect enlargement

To cite this article: Bowen Zheng and Grace X Gu 2020 *Nanotechnology* **31** 085707

View the [article online](#) for updates and enhancements.



IOP | ebooks™

Bringing you innovative digital publishing with leading voices to create your essential collection of books in STEM research.

Start exploring the [collection](#) - download the first chapter of every title for free.

Recovery from mechanical degradation of graphene by defect enlargement

Bowen Zheng and Grace X Gu 

Department of Mechanical Engineering, University of California, Berkeley, CA 94720, United States of America

E-mail: ggu@berkeley.edu

Received 3 September 2019, revised 8 October 2019

Accepted for publication 4 November 2019

Published 28 November 2019



CrossMark

Abstract

The extraordinary properties of graphene have made it an elite candidate for a broad range of emerging applications since its discovery. However, the introduction of structural defects during graphene production often compromises the theoretically predicted performance of graphene-based technologies to a great extent. In this study, a counterintuitive defect enlargement strategy to recover from defect-induced mechanical degradation is explored, of which the realization may lead to an enhanced operating efficiency and manufacturing feasibility. Our molecular-dynamics simulation results show that the enlargement of a preexisting defect to an elliptical shape can potentially recover from the mechanical degradation that the very defect has caused. For a defective graphene sheet having a failure strain of 48% of the pristine graphene sheet, enlarging the defect can enhance the failure strain up to 80% of the pristine graphene sheet. The mechanism of degradation recovery lies in a reduced change in curvature during deformation, which is further solidified by theoretical quantification and stress-field analysis. This theory can also predict and pinpoint the location of the initiation of the fracture—where the curvature changes most significantly during the deformation. In addition, the influence of an elliptical defect on the mechanical properties of a graphene sheet is systematically studied, which is not well understood today. Finally, the degradation recovery potential of defect of various sizes is examined, showing that the initial defect that can create the highest degree of geometric asymmetry has the best potential for degradation recovery. This study investigates the recovery from defect-induced mechanical degradation and the influence of elliptical defects on the mechanical properties of a graphene sheet, which widens our understanding of the possibility of fine-tuning mechanical properties via defect engineering and has the potential to improve materials for emerging technologies such as supercapacitor devices.

Keywords: graphene, molecular dynamics, defects, mechanical properties, fracture

(Some figures may appear in colour only in the online journal)

1. Introduction

The discovery of graphene [1] has profoundly boosted the development of scientific research and a broad range of engineering applications due to its extraordinary electronic [2–4], thermal [5, 6], and mechanical [7–11] properties. Despite being a one-atom thick 2D material, monolayer graphene possesses an exceptional combination of mechanical properties including an ultrahigh Young's modulus of ~ 1 TPa [7] and an unsurpassed intrinsic tensile strength of 130 GPa [7]. These mechanical properties not only make graphene ideal for advanced ultra-strong nanocomposites [12–15], but also make it an elite

candidate for cutting-edge technologies such as micro-/nano-electromechanical systems (M-/N-EMS) [16, 17], supercapacitor devices [18, 19], stretchable electronics [20, 21], among others. The superlative mechanical properties of graphene and the rapid development of experimental and numerical approaches have given rise to the advances in graphene mechanics [15, 22–25]. For example, scientific communities are becoming more and more interested and knowledgeable in the 3D behavior of the 2D material. Due to the atomic-thin nature, graphene possesses an ultra-low bending rigidity, which enables a vast tuning space of out-of-plane behavior such as rippling [26–28] and 3D folding [29–31].

Another area of interest is the mechanics of defective graphene. During the graphene production processes such as mechanical exfoliation [32, 33] and chemical vapor deposition (CVD) [34, 35], it is not uncommon that a variety of structural defects can be introduced including point defects, dislocations, and grain boundaries, which strongly affect the electronic, thermal, and mechanical properties of graphene. Also, the mobile nature of defects profoundly enriches the roles that these defects can play. Defect behavior in graphene has received great attention in the recent years [24]. The influences of vacancies, charged impurities, and local distortions on the electronic properties of mechanically strained graphene sheets have been systematically discussed by researchers, showing that electronic properties such as the electronic density of states are highly sensitive to (and therefore tunable by) these defects [36–38]. A recent study proposed a concept of graphene straintronics to induce a large electronic bandgap by tensile and shear strains, which may contribute to a sizeable and robust electronic energy gap in nanoelectronic devices [39]. On many occasions, the realization of the full potential of graphene requires it to be in a state that is defect-free or defect-scarce. It is because the presence of defects can compromise the theoretically predicted or lab-measured properties to a great extent, resulting in the deteriorated operating efficiency of graphene-based applications. A few theoretical and numerical endeavors have explored the influence of defects on the mechanical properties of graphene, showing that strength and stiffness losses are generally proportional to the defect size and concentration, and are also affected by temperature and chirality [40–43]. Zandiashbar *et al* studied the effect of various types of defects on the strength and stiffness of graphene, showing that although the mechanical properties of graphene can exhibit a significant drop in the presence of vacancies, strength and stiffness show little degradation when graphene bears sp^3 -type defects [44]. However, these types of defects are intrinsically different from each other and therefore have a fundamentally different impact on the mechanical properties of graphene. Is it possible to recover from defect-induced mechanical degradation by counterintuitively enlarging the defect (instead of miniaturizing the defect) and without changing the type of defect? A positive answer to this question has at least two constructive indications. For one, degradation recovery by enlarging the defect reduces the number of atoms in the system while improving the performance, which tremendously enhances the efficiency as a result. For another, enlarging the defect does not involve switching the type of defect and removes material instead of adding to the material, which makes it possible to modify the defective graphene as it is rather than remaking graphene from scratch again.

In this study, the possibility of recovering from defect-induced mechanical degradation by enlarging the defect is explored via molecular dynamics (MD) simulations. Graphene sheets centered on a circular defect of variable radius are used as the initial defective graphene sheets. Enlargement modifications are made onto the preexisting circular defect aiming to achieve degradation recovery. Mechanical properties of interest include failure stress, failure strain, and mode of fracture initiation. These properties of initial defective graphene sheets and various modified graphene sheets are calculated and compared against a

pristine graphene sheet to evaluate the recovery effect. Deformation characteristics of effective recovery are examined to shed light on the counterintuitive recovery mechanism. The influence of elliptical defects on the mechanical properties of graphene sheets is systematically studied, which has not been adequately discussed in the literature thus far. Finally, the degradation recovery potential with respect to various defect sizes is discussed to obtain an estimation of expected recovery given the information of preexisting defects. The investigation of mechanical degradation recovery by counterintuitive defect enlargement may open up new defect engineering possibilities to improve the performance and manufacturing feasibility of 2D material-based nanotechnologies.

2. System description and MD simulation setup

Because in real-world applications graphene-based materials may be subject to mechanical loadings in random directions, when studying in-plane mechanical properties of graphene, it is crucial to take into account both the zigzag and armchair directions based on which random loadings can be decomposed. To this end, the square-shaped monolayer graphene sheet is chosen to study for comparison between the two orthogonal directions. A schematic of the pristine graphene sheet is provided in figure 1(a) with tensile loading directions being illustrated. The graphene sheet has a side length of $L \sim 110 \text{ \AA}$ and consists of 4966 atoms when no defect is present. It has been shown that when the diagonal length of graphene sheet is over 5 nm, the size effect of the model size can be largely neglected [45]. The length of covalent C–C bond in the initial configuration is 1.421 Å. Based on a deformation-control manner, in-plane tensile loading is applied by assigning displacement at a constant speed to a 3 Å wide stripe at one end (shaded area in figure 1(a)), while a 3 Å wide stripe at the other end is held immobile in all three dimensions. A strain rate of 10^9 s^{-1} is used in all loading scenarios [45]. The defects studied in this paper are circular and elliptical porous defects representing vacancy clusters of various sizes and shapes. To simplify the problem, defects are located at the center of the graphene sheet. Graphene sheets with a centered elliptical defect of various sizes and shapes are shown in figure 1(b), parametrized by the length of semi-axis in the zigzag direction a and the length of the semi-axis in armchair direction b . As a special case, the elliptical defect degenerates to a circular defect when $a = b = R$, where R is the defect radius.

MD simulations are conducted using the open-source MD package LAMMPS (Large-scale Atomic/Molecular Massively Parallel Simulator) [46]. To capture the bond-breaking and reforming behaviors that play a pivotal role in the material failure process, an Adaptive Intermolecular Reactive Empirical Bond Order (AIREBO) potential [47] is used to compute the interactions between pairs of carbon atoms. Consisting of a REBO term to model short-ranged interaction and a Lennard-Jones (LJ) term to model long-ranged interaction, the AIREBO potential can be formulated as

$$E = \frac{1}{2} \sum_i \sum_{j \neq i} (E_{ij}^{\text{REBO}} + E_{ij}^{\text{LJ}}) \quad (1)$$

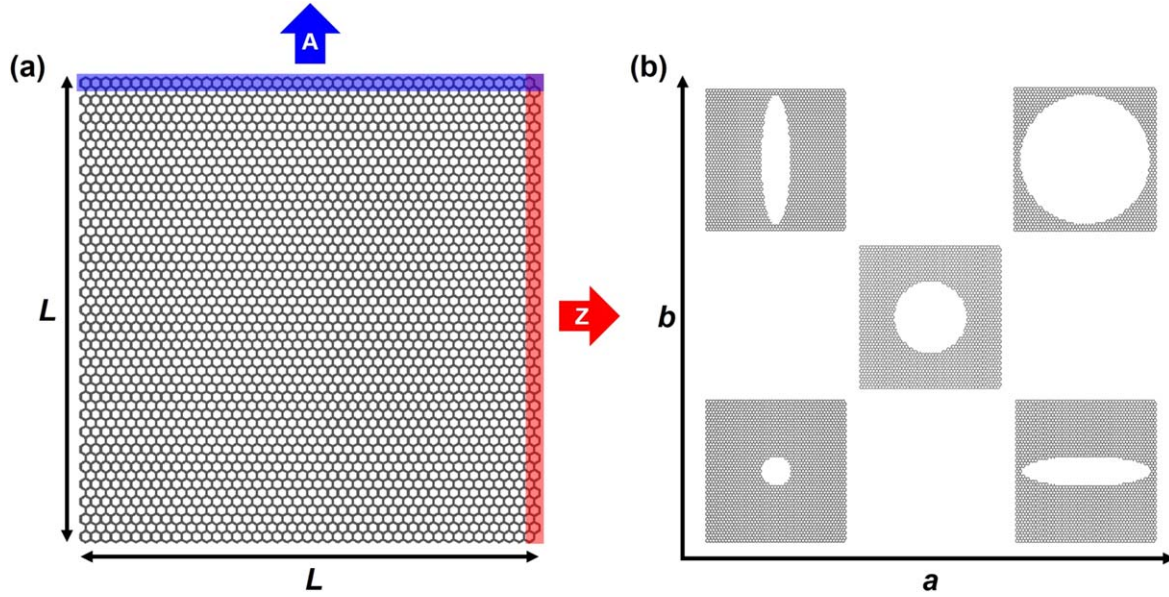


Figure 1. Schematic of pristine and defective graphene sheets used for MD simulation. (a) Square pristine graphene sheet and illustration of tensile loading directions. Arrows with ‘Z’ and ‘A’ represent tensile loading in the zigzag and armchair directions, respectively. (b) Square graphene sheets with an elliptical defect of various sizes and shapes.

where E is the total potential energy contributed by all atomic interactions, and E_{ij}^{REBO} , E_{ij}^{LJ} represent the REBO potential and the LJ potential between atoms i and j , respectively. The REBO term has two cutoff distances in the switching function that controls the bond-breaking behavior, which are 1.7 Å and 2.0 Å, respectively, by default [47]. Here, the smaller cutoff distance is

where i and j take on x , y , or z to generate the six components of the symmetric tensor; m^α and v^α are the mass and velocity of atom α ; $r_{\alpha\beta}$ and $f_{\alpha\beta}$ are the distance and force between atoms α and β . After the calculation of stress tensor on each individual atom, the equivalent stress σ of a graphene sheet is calculated based on von Mises stress

$$\sigma = \sqrt{\frac{1}{2}[(\sigma_{xx} - \sigma_{yy})^2 + (\sigma_{yy} - \sigma_{zz})^2 + (\sigma_{zz} - \sigma_{xx})^2 + 6(\sigma_{xy}^2 + \sigma_{yz}^2 + \sigma_{zx}^2)]} \quad (3)$$

changed to 1.92 Å to simulate the mechanical behavior of graphene more accurately with benchmarking density functional theory calculations, a modification which has been used and validated by many previous studies [48–51]. The cutoff distance of the long-ranged LJ term is set to 6.8 Å. The integration time step is set as 1 fs. Periodic boundary conditions are used in two in-plane dimensions and a fixed boundary condition is applied to the perpendicular out-of-plane dimension. An ensemble of random velocity corresponding to the temperature $T = 300$ K is firstly generated throughout the system. Then an equilibrium is realized by running a simulation in the isothermal-isobaric (NPT, where the number (N) of particles, system pressure (P) and temperature (T) are maintained as constants) ensemble with a Nose–Hoover thermostat [52] at the same temperature for 50 ps, where the maximum out-of-plane fluctuation is ~ 2 Å. The loading scenario is simulated in the canonical (NVT, where the number (N) of particles, system volume (V) and temperature (T) are maintained as constants) ensemble at $T = 300$ K. The method of stress calculation is described below. The stress tensor S_{ij}^α for atom α is firstly calculated by the following equation:

$$S_{ij}^\alpha = \frac{1}{2}m^\alpha v_i^\alpha v_j^\alpha + \sum_{\beta=1}^n r_{\alpha\beta}^j f_{\alpha\beta}^i \quad (2)$$

where

$$\sigma_{ij} = \frac{1}{V_0} \sum_{\gamma=1}^n S_{ij}^\gamma$$

where $V_0 = L^2 t_e$ is the initial volume, and $t_e = 3.35$ Å is the equivalent thickness of monolayer graphene [53].

3. Results and discussion

Firstly, MD simulations are conducted to investigate the mechanical properties of the following graphene sheets in the zigzag direction as a set of demonstrative examples: (a) pristine graphene sheet as a benchmark, (b) graphene sheet with a circular defect with a radius $R = 0.1L$ as a representative defective graphene sheet, and (c) graphene sheet with an elliptical defect with a parameter pair $(a, b) = (0.45L, 0.1L)$ representing an enlarged circular defect in the zigzag direction only with the purpose of degradation recovery. The vacancy concentration of the representative defective graphene with a circular defect is $\sim 3\%$, which closely resembles graphene in an experimental setting [54], as well as other simulation studies [41, 55]. Here, the mechanical properties of interest are failure

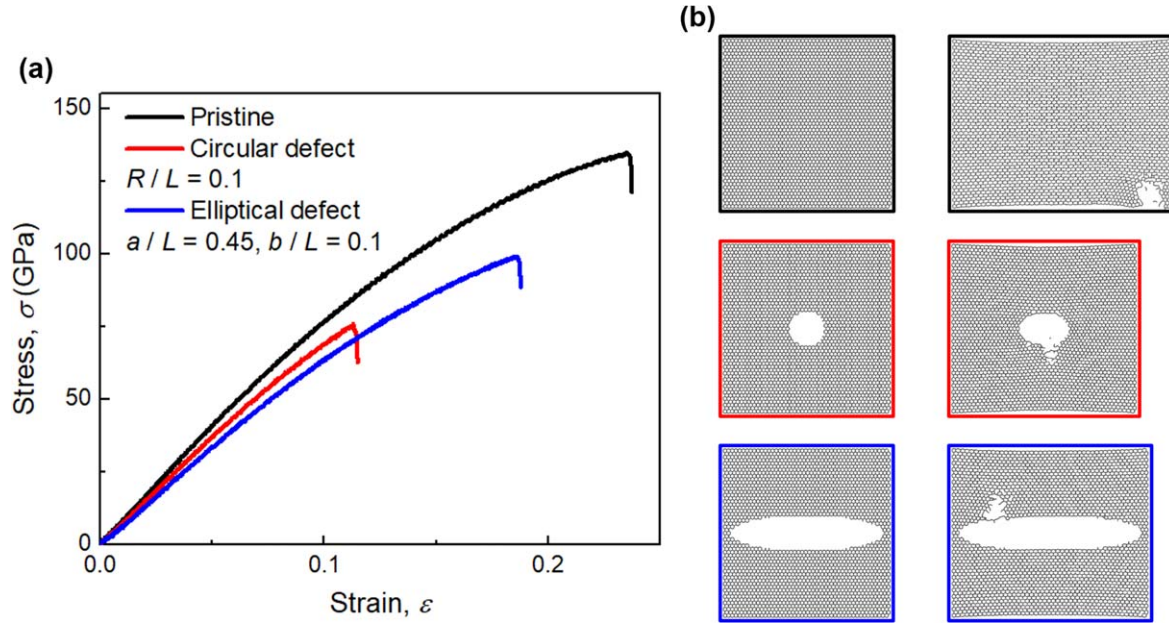


Figure 2. Demonstration of degradation recovery by enlarging the preexisting defect to an elliptical shape. (a) Calculated stress–strain curves, and (b) unloaded and failure morphologies of a pristine graphene sheet, graphene sheet with a circular defect, and graphene sheet with an elliptical defect for degradation recovery.

stress, failure strain, and mode of fracture initiation. The calculated stress–strain curves of the above three graphene sheets subject to loading in the zigzag direction are presented in figure 2(a). Comparing a graphene sheet with a circular defect with a pristine graphene sheet, failure stress and failure strain are lowered, suggesting mechanical degradation. However, a graphene sheet with an elliptical defect, despite bearing a larger defect compared to the circular defect, possesses a much higher failure stress and failure strain, suggesting a profound recovery effect. The mechanical properties of the above three graphene sheets are summarized below. Failure stress can be recovered from 56.4%–73.6% σ_P and failure strain can be recovered from 47.9%–79.3% ε_P , where $\sigma_P = 134.6$ GPa and $\varepsilon_P = 0.235$ are the failure stress and failure strain of a pristine graphene sheet, respectively. The modes of fracture initiation of the three graphene sheets are provided in figure 2(b). For a pristine graphene sheet, fracture initiates at the edge close to the loaded region; for a graphene sheet with circular defects, fracture occurs in the middle part of the arc; for graphene with elliptical defects, fracture initiates from along the arc close to the vertex of the defect where the most dramatic change in curvature happens during the deformation process. These differences in failure mode may provide valuable insights into the mechanism of degradation recovery.

To cast light on the mechanism of the degradation recovery via counterintuitive defect enlargement, the maximum deformation before the fracture is examined. To this end, morphologies of the surrounding areas of circular with a radius $R = 0.1L$ and elliptical defects with $(a, b) = (0.45L, 0.1L)$ right before failure are shown in figure 3(a) to present the maximum deformation with the red arcs representing the defect rims in unloaded conditions. As can be observed, graphene with a circular defect, though having a lower failure strain, shows a

much more drastic deformation at the defect rim compared to graphene with an elliptical defect before the onset of fracture, which can be characterized by a change in curvature on the defect rim. It is hypothesized that enlarging the circular defect to an elliptical shape reduces the change in curvature when the graphene sheet is loaded to a certain amount of strain, which leads to a mediated deformation process and a postponed onset of fracture, and ultimately results in enhanced failure strain. In addition, failure initiates from the point on the defect rim having the maximum change in curvature. To test the hypothesis quantitatively, the curvature at any given stretching strain is formulated as follows. The lengths of both semi-axes of the elliptical defect are subject to change as the graphene sheet is stretched, which can be expressed as $a(\varepsilon) = a_0(1 + \varepsilon)$ and $b(\varepsilon) = b_0(1 - \nu\varepsilon)$. Here, a_0 and b_0 are the prescribed lengths of the semi-axes of the elliptical defect in the zigzag and arm-chair directions in the unloaded graphene. ν is defined as the ratio of the amount of shrinkage of the elliptical defect transversely to the loading to the amount of lengthening in the loading direction, similar to the concept of Poisson's ratio. ν is assumed to be independent of strain ε and ranges from 0–1. The curvature κ at a certain point on the defect rim ($a \cos t, b \sin t$) at any moment during the loading process can be expressed as

$$\begin{aligned} \kappa(\varepsilon, t) &= a(\varepsilon)b(\varepsilon)(a^2 \sin^2 t + b^2 \cos^2 t)^{-\frac{3}{2}} \\ &= a_0 b_0 (1 + \varepsilon)(1 - \nu\varepsilon)(a_0^2(1 + \varepsilon)^2 \\ &\quad \times \sin^2 t + b_0^2(1 - \nu\varepsilon)^2 \cos^2 t)^{-\frac{3}{2}}. \end{aligned} \quad (4)$$

The curvature on defect rim in the unloaded state κ_0 can be expressed as

$$\kappa_0(t) = a_0 b_0 (a_0^2 \sin^2 t + b_0^2 \cos^2 t)^{-\frac{3}{2}}. \quad (5)$$

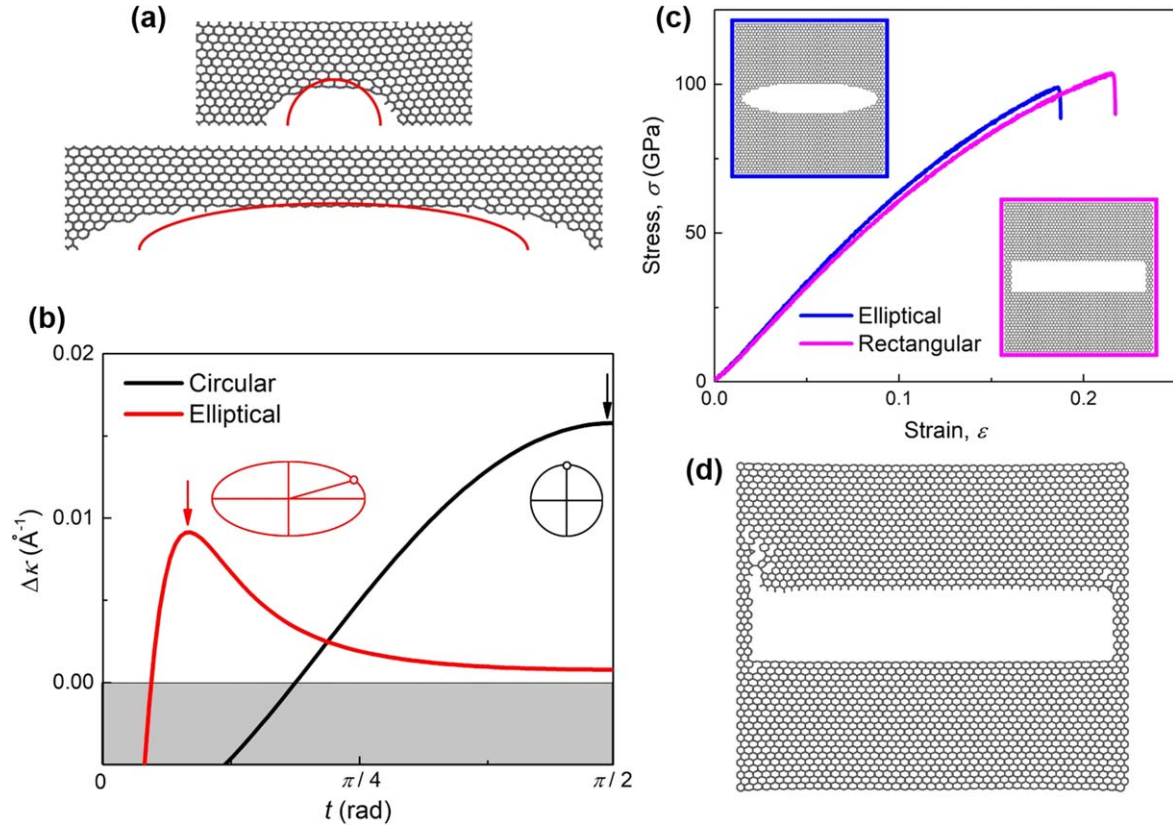


Figure 3. Illustration of proposed recovery mechanism and its validation. (a) Morphologies of surrounding areas of circular and elliptical defects right before fracture. Red arcs show the defect rims before the loading. (b) Change in curvature at any point on the rim of the circular and the elliptical defect, where the arrows point to the maximum changes in curvature in the two cases. (c) Stress–strain curves of graphene sheets with the elliptical defect and the rectangular defect of the same dimensions in the zigzag and armchair directions. (d) Mode of fracture initiation of graphene sheets with the rectangular defect.

Note that the tear-like deformation that results in the failure around the defect in fact corresponds to a decrease in curvature. Therefore, we inverse the sign of the change in curvature to be

$$\begin{aligned} \Delta\kappa(\varepsilon, t) = & -[\kappa(\varepsilon, t) - \kappa_0(t)] = a_0 b_0 [(a_0^2 \sin^2 t \\ & + b_0^2 \cos^2 t)^{-\frac{3}{2}} - (1 + \varepsilon)(1 - \nu\varepsilon) \\ & \times (a_0^2 (1 + \varepsilon)^2 \sin^2 t + b_0^2 (1 - \nu\varepsilon)^2 \cos^2 t)^{-\frac{3}{2}}]. \end{aligned} \quad (6)$$

We use the approximation $1 - \nu\varepsilon \approx 1$. Now equation (6) becomes

$$\begin{aligned} \Delta\kappa(\varepsilon, t) \cong & a_0 b_0 [(a_0^2 \sin^2 t + b_0^2 \cos^2 t)^{-\frac{3}{2}} \\ & - (1 + \varepsilon)(a_0^2 (1 + \varepsilon)^2 \sin^2 t + b_0^2 \cos^2 t)^{-\frac{3}{2}}]. \end{aligned} \quad (7)$$

Because of the symmetry of the defect geometry, only the range $0 \leq t \leq \pi/2$ is considered. For the circular and elliptical defects in figure 3(a), results based on equation (7) can not only demonstrate the reduction of the maximum change in curvature by the defect enlargement, but it can also predict and pinpoint the location of the onset of failure in both cases. Plugging in equation (7) $a_0 = b_0 = 0.1L$ for the circular defect and $a_0 = 0.45L$, $b_0 = 0.1L$ for the elliptical defect and set the stretching strain $\varepsilon = 0.1$, the change in curvature at any point on the rim of the defect can be obtained, as is shown in figure 3(b). For the circular defect, the maximum change in

curvature occurs at the vertex on the semi-axis transverse to the loading ($t = \pi/2$), while for the elliptical defect, the location of the maximum change in curvature moves toward the vertex perpendicular to the loading ($t = 0.17 \times \pi/2$). These predicted locations are in good agreement with the initiation of failure presented in figure 2(b). Additionally, the maximum change in curvature is substantially lowered by expanding the circular defect to an elliptical shape. The curves shown in figure 3(b) also capture the portion of the defect rim that exhibits tear-like deformation ($\Delta\kappa > 0$), the portion that exhibits contraction-like deformation ($\Delta\kappa < 0$), and the point on the rim not subject to any change in curvature ($\Delta\kappa = 0$).

To further validate the proposed degradation recovery mechanism based on the change in curvature, a graphene sheet with a rectangular defect of the same dimensions in the zigzag and armchair directions as the elliptical defect is simulated. A rectangular defect produces an even smaller change in curvature compared to an elliptical defect and should therefore have higher failure strain. Figure 3(c) presents the stress–strain curves of graphene sheets with an elliptical and rectangular defect, which confirms the hypothesis by showing that the graphene sheet with a rectangular defect has a higher failure stress and strain. It is also noteworthy in figure 3(d) that for a graphene sheet with a rectangular defect, fracture initiates at one of the vertices where the curvature changes more significantly than at any other

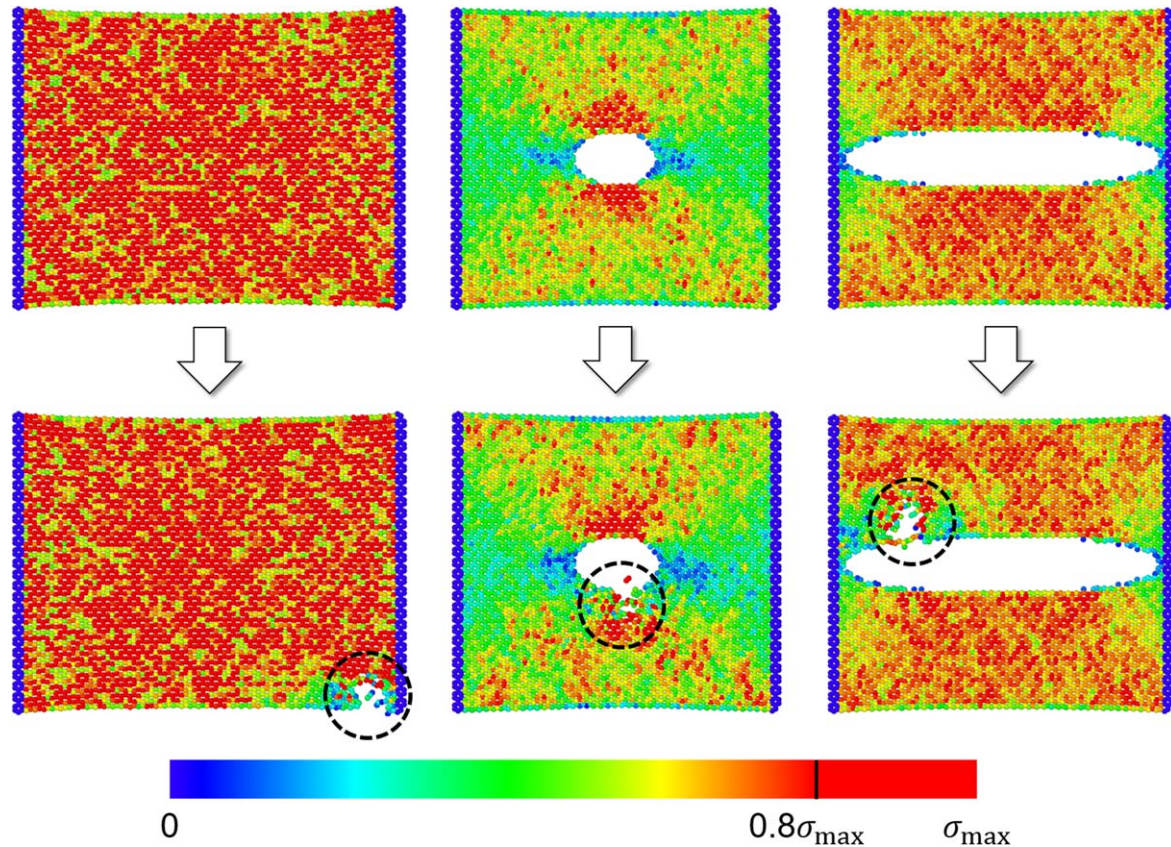


Figure 4. Stress distributions during the failure process of pristine graphene sheets and graphene sheets with circular and elliptical defects. To illustrate the stress concentration more clearly, stress that is over 80% of the maximum stress σ_{\max} of the individual case is colored red.

point along the defect, which again supports the proposed mechanism. This observation also adequately explains the fracture initiation mode of a pristine graphene sheet: fracture initiates at the edge close to the loaded region where the curvature changes fastest. To further solidify the proposed theory related to the change in curvature, stress distributions during the failure process of pristine graphene sheet, graphene sheets with circular and elliptical defects are supplemented, as is shown in figure 4. To illustrate the stress concentration more clearly, stress that is over 80% of the maximum stress σ_{\max} of the individual case is colored red. As can be seen, for graphene with a circular defect, stress over $0.8\sigma_{\max}$ is distributed in a more localized fashion compared to graphene with an elliptical defect. This phenomenon indicates that the latter utilizes a graphene sheet in a more efficient way where atoms are better involved in the deformation during the loading process, thus having a higher failure stress and strain. Furthermore, it is notable that fracture initiates in the area with high stress which is also associated with the maximum change in curvature on the defect rim. Hence, this observation is consistent with and solidifies the proposed mechanism.

Following the demonstration and reasoning of the degradation recovery capability by forming an enlarged elliptical defect, the influences of how long the defect is lengthened in the examined direction and the possible difference between the examined directions are discussed. In the discussion below, defects are lengthened in either the zigzag

or armchair direction starting from a centered circular defect with a radius $R = 0.1L$. Figures 5(a) and (b) show the failure stress when the defect is lengthened in the examined direction with the perpendicular dimension fixed. As can be seen, both failure stress and failure strain are enhanced as the length of the elliptical defect in the examined direction increases, and no fundamental difference is shown when the zigzag or armchair direction is examined. The stable growth can be associated with the proposed recovery mechanism, where the change in curvature is gradually reduced as the dimension of the defect in the examined direction increases. Because graphene is an intrinsically anisotropic material, it is interesting to look at the influence of 1D lengthening on the mechanical anisotropy of a graphene sheet by examining mechanical properties in the zigzag and armchair directions at the same time. A 2D $\ln(\varepsilon_{F,Z}/\varepsilon_{F,A})$ -versus- $\ln(\sigma_{F,Z}/\sigma_{F,A})$ anisotropy graph is proposed to quantify the anisotropic property of the graphene sheet with respect to both failure stress and failure strain. The evolutionary paths in figure 5(c) show that the mechanical anisotropy of graphene sheets can be concretely intensified going from a circular to an elliptical defect in both the zigzag and armchair directions.

Having investigated the effect of 1D lengthening of a circular defect to an elliptical defect, the influence of size and shape of elliptical defect on the mechanical properties of graphene sheet are systematically discussed with 2D variable parameter pair (a, b) . Simulation results of $8 \times 8 \times 2 = 128$

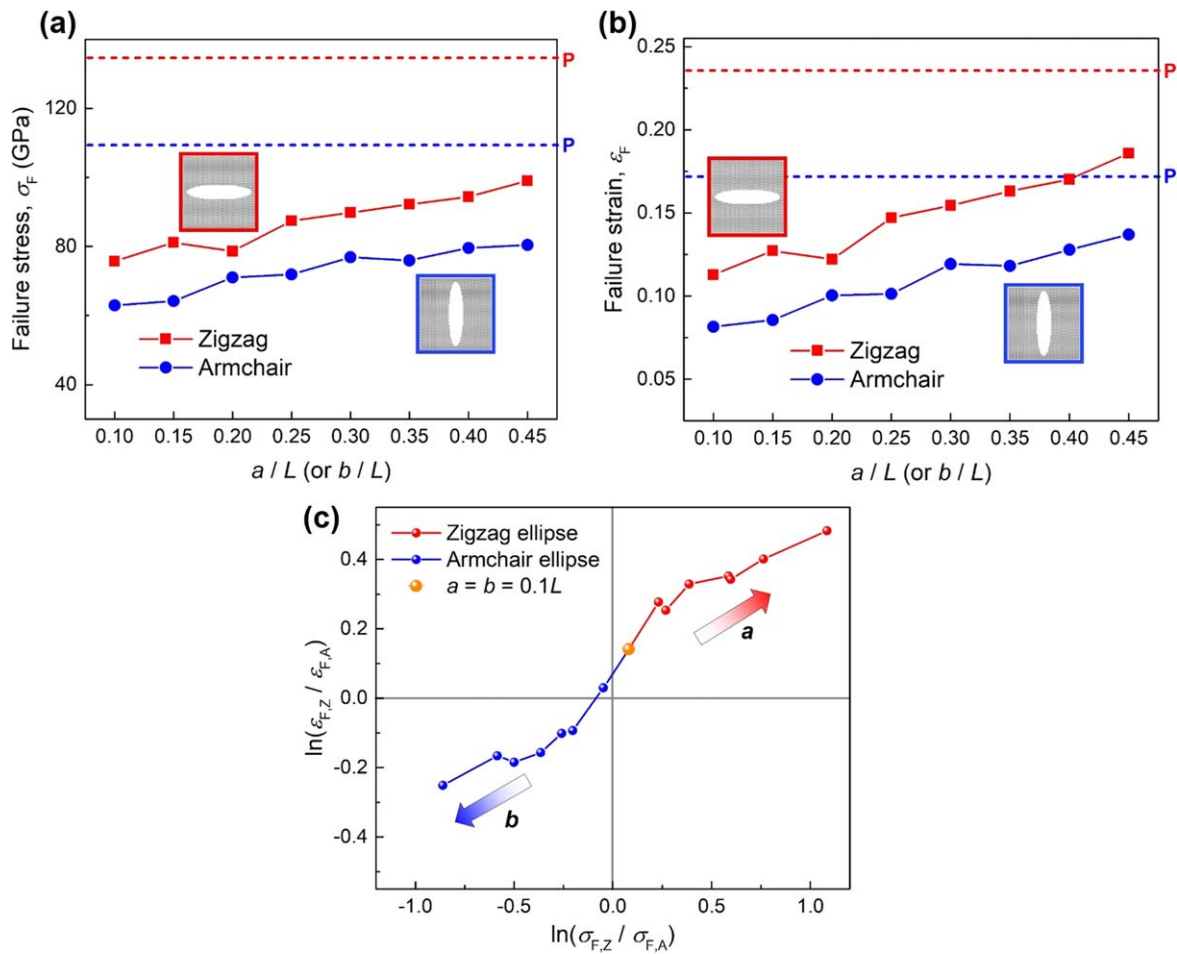


Figure 5. The influence of 1D lengthening of a circular defect on the mechanical properties of graphene sheet. (a) Failure stress and (b) failure strain of graphene sheet with a defect of increasingly lengthened dimension parallel to the loading and unchanged dimension in the perpendicular direction. The failure stress and strain of a pristine graphene sheet are added on the figures for comparison, as are marked with dashed-horizontal lines and the letter 'P'. (c) Evolutionary path of data points on the 2D anisotropy graph as the axis of the elliptical defect in the examined direction is lengthened, while the axis perpendicular to the examined direction is fixed.

instances of graphene sheets with elliptical defect in the zigzag and armchair directions are conducted, where a/L , $b/L \in [0.10, 0.15, \dots, 0.45]$. Figures 6(a) and (b) show the influence of size and shape on failure stress in the zigzag and armchair directions, and figures 6(c) and (d) show the influence on failure strain. The recovering effect and the weakening effect of the defect dimension perpendicular to the examined direction are illustrated with green and blue arrows pointing to the direction of greater intensity. White lines represent circular defects where $a = b$, of which the failure stress and strain as a function of defect radius R are presented in figures 6(e) and (f). Observations and corresponding conclusions based on these figures are provided as below.

- i. In the zigzag direction, the maximum failure stress and strain are achieved when the zigzag dimension a is large and the armchair dimension b is small, while in the armchair direction, failure stress and strain reach their maximum in concord when the armchair dimension b is large and the zigzag dimension a is small. Therefore, for a graphene sheet with ellipse-shaped vacancy defect

cluster, the defective graphene sheet obtains its best mechanical properties when the elliptical defect has a long axis in the examined direction while having a short axis perpendicular to the examined direction. This result goes against the intuition that a smaller defect produces higher strength and ductility.

- ii. Although an elliptical defect with a long axis in the examined direction and a short axis in the perpendicular direction strengthens the examined direction best, this configuration weakens the unexamined direction and intensifies the mechanical anisotropy most, corresponding to the discussion in figure 5(c).
- iii. According to the parametric results of a circular defect in figures 6(e) and (f), as the radius of the circular defect increases, failure stresses in both directions decrease monotonously, while failure strains change insignificantly. In addition, no recovering effect is observed with the defect being enlarged. Hence, it can be concluded that the recovery effect of elliptical defects is contributed by the geometric asymmetry of defect clusters. Furthermore, this result strengthens the theory

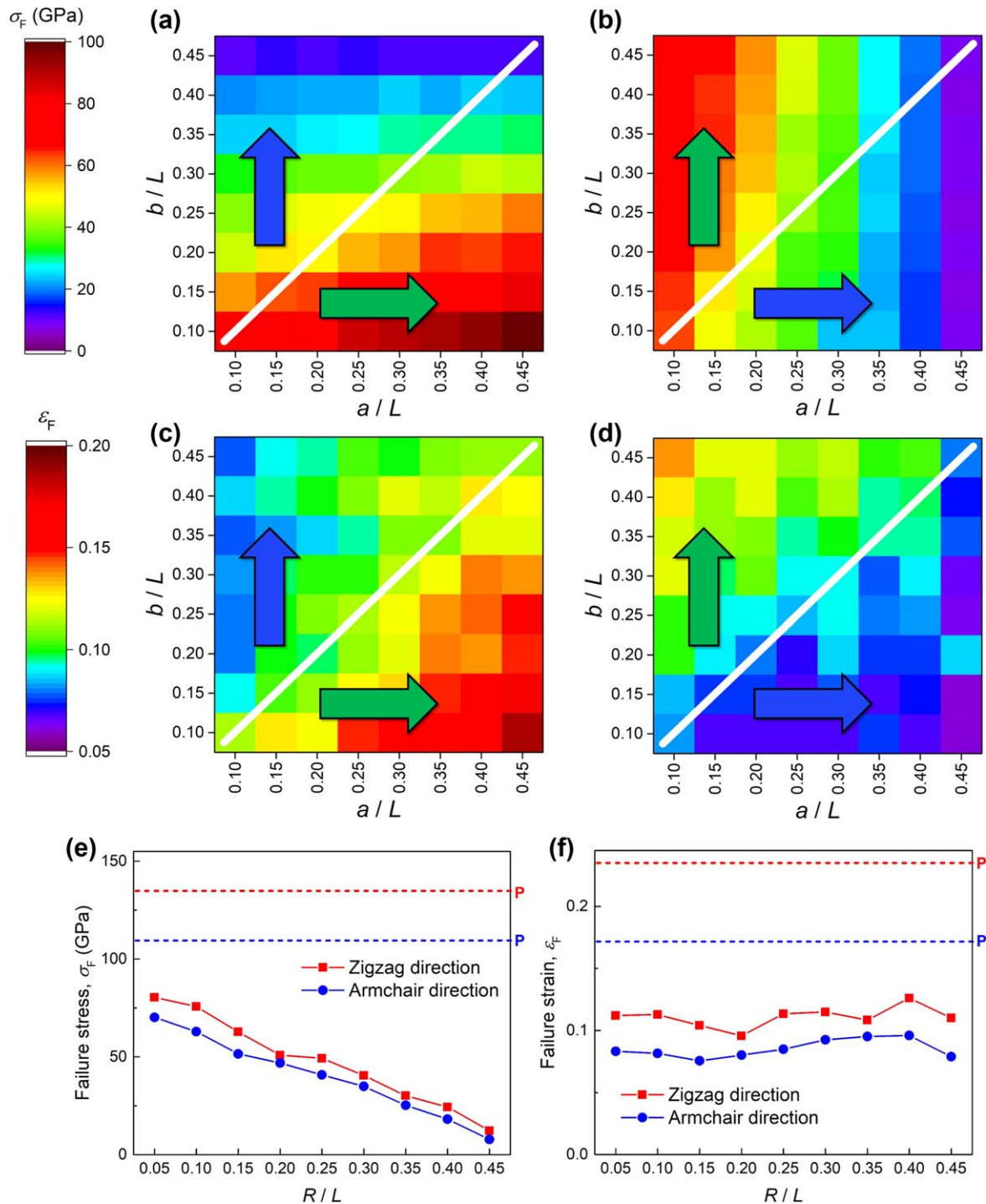


Figure 6. The influence of size and shape of an elliptical defect on the mechanical properties of graphene sheet. Failure stress maps of graphene sheet with elliptical defects of various sizes and shapes in the (a) zigzag and (b) armchair directions. Failure strain maps of a graphene sheet with elliptical defects of various sizes and shapes in the (c) zigzag and (d) armchair directions. Recovering effect and the weakening effect of the defect dimension perpendicular to the examined direction are illustrated with green and blue arrows pointing to the direction of greater intensity. White lines represent circular defects. The influence of circular defects on (e) failure stress and (f) failure strain of graphene sheet. The failure stresses and strains of pristine graphene sheet are added on the figures for comparison, as are marked with dashed-horizontal lines and the letter 'P'.

of change in curvature because enlarging the circular defect does not change the curvature therefore no early or postponed fracture initiation is caused. This suggests a new design strategy of decoupling failure stress and failure strain.

Having systematically studied the influence of size and shape of an elliptical defect as well as the degenerated scenario of a circular defect, the potential of recovery from defect-induced mechanical degradation by circular defects of various sizes is discussed. The failure strains of pristine

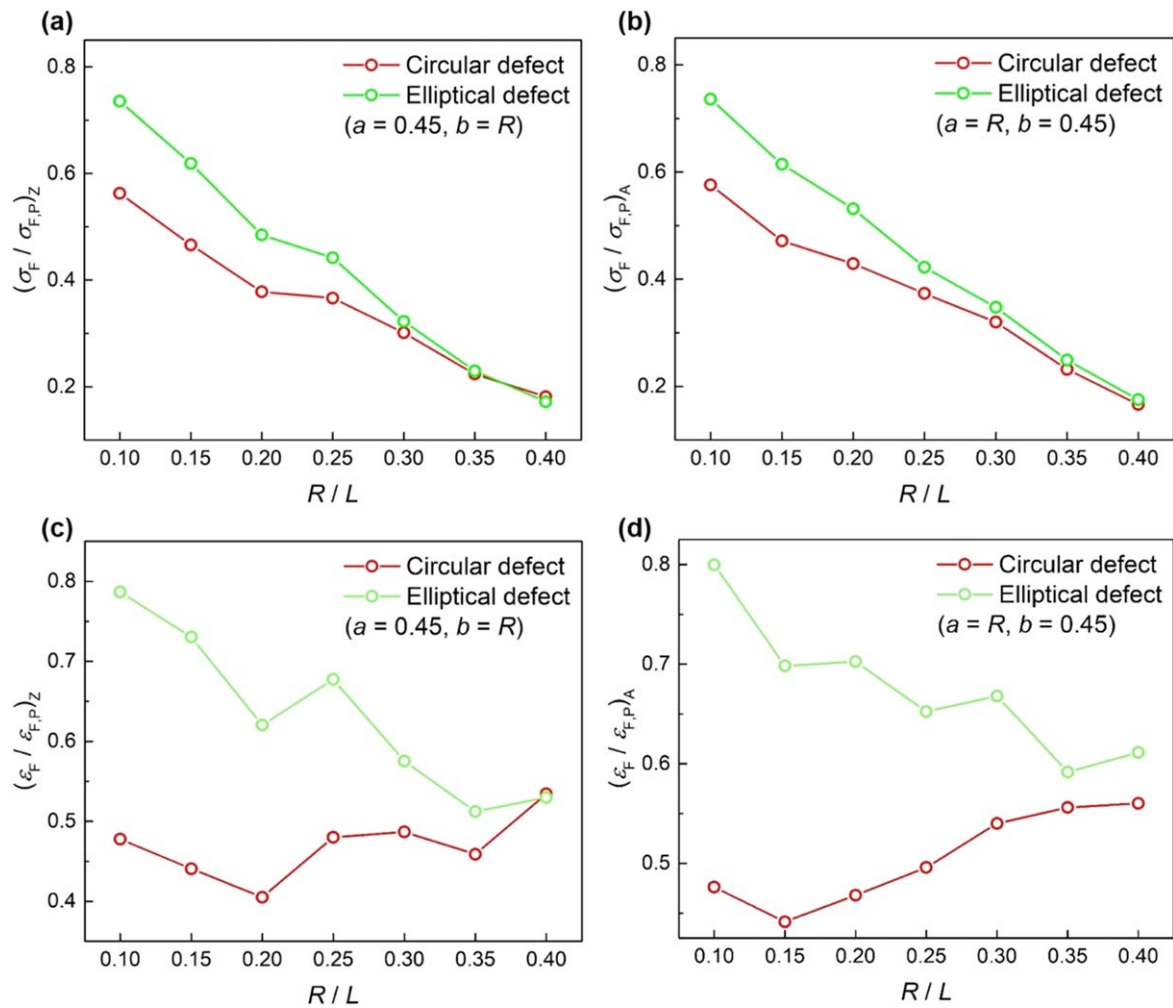


Figure 7. Evaluation of recovery potential with respect to variable size of a circular defect. Failure stress in the (a) zigzag and (b) armchair directions. Failure strain in the (c) zigzag and (d) armchair directions.

graphene in the zigzag and armchair directions are used as a benchmark to normalize the failure strains of circular and elliptical defects. An evaluation of the recovery potential of failure stress and strain with a variable radius of circular defects is provided in figure 7, where in the examined direction the axis is lengthened to $2 \times 0.45L$. It is observed that the recovery potential decreases as the circular defect becomes larger and that the recovery effect is in general closed when the diameter reaches $0.4L$. This phenomenon can be explained by the fact that the maximum geometric asymmetry of the defect is reduced by the size of the defect. Comparing the results in figure 7, failure strain has a higher recovery capability than failure stress and the effect on the zigzag and armchair directions are similar. To investigate the opening of a recovery effect, we create the smallest vacancy in graphene by removing one atom at the center and also create a line defect with a length of $0.5L$ extended from the one-atom vacancy. Figure 8 shows that the 1D enlargement of the one-atom vacancy exhibits a recovery effect, suggesting that there appears to be no threshold for opening a recovery effect.

To address the issue of strengthening one direction at the expense of weakening the other, the prescribed circular defect is expanded to a square shape to pursue enhanced mechanical

performance in both the zigzag and armchair directions. The diameter of the circular defect and the side length of the square defect are both chosen as $0.15L$. Stress-strain relations of the above defective graphene in two directions are presented in figure 9. As is shown, by expanding the circular defect to the smallest square defect, the mechanical properties in both directions can be enhanced.

4. Concluding remarks

In this paper, the possibility of recovering from defect-induced mechanical degradation by enlarging the defect is explored via MD simulation. It is shown that the enlargement of the preexisting defect to an elliptical shape has a counterintuitive potential to recover from the mechanical degradation that the very defect has caused. The significance of this finding has two main implications. Firstly, degradation recovery by enlarging the defect reduces the atoms of the system while improving the performances, which tremendously enhances the efficiency. Secondly, enlarging the defect does not involve switching the type of defect and removes material instead of adding, thus increasing the

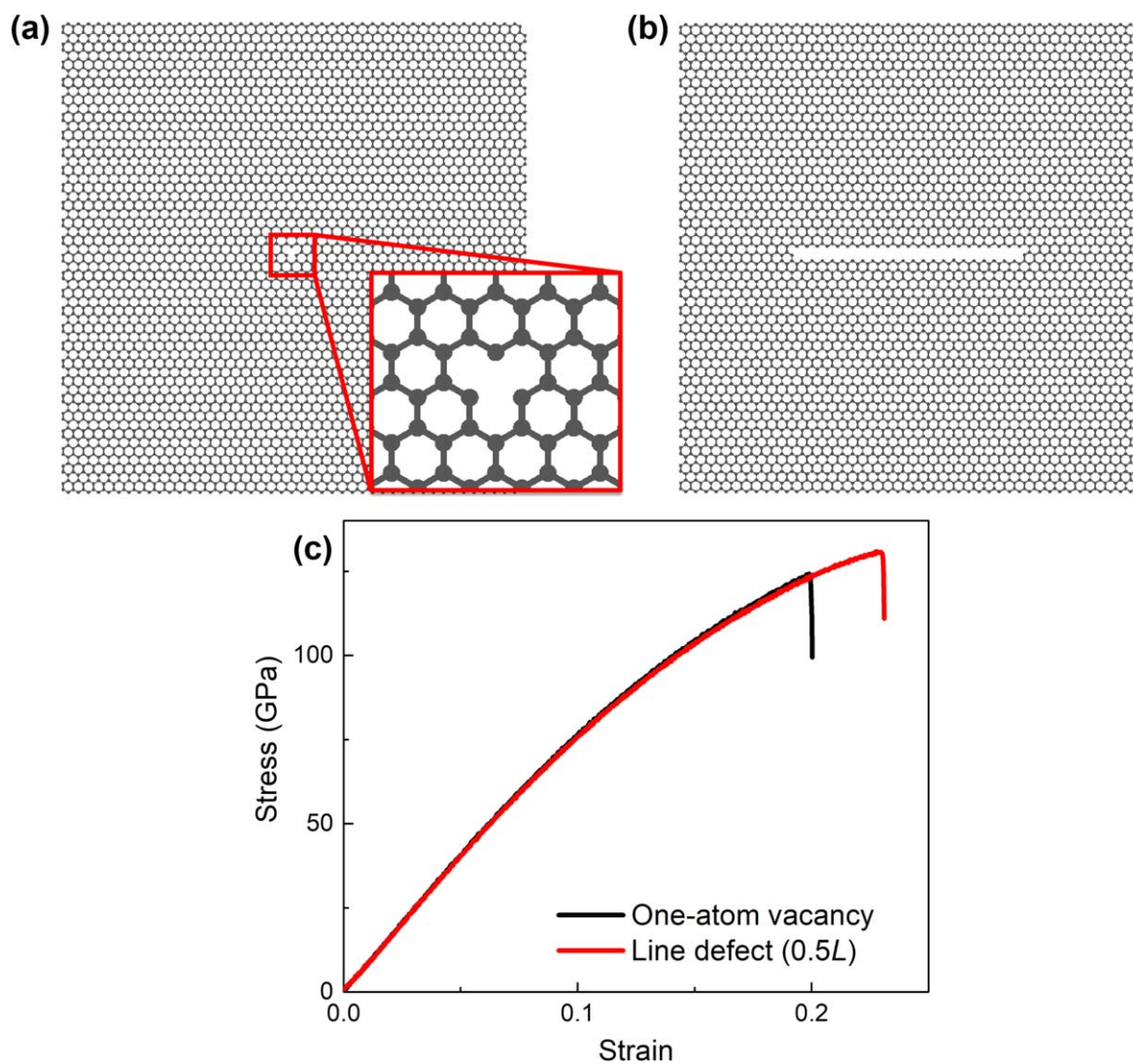


Figure 8. Graphene sheets containing one-atom vacancy and its corresponding line defect. Geometries of graphene with (a) the one-atom vacancy and (b) the line defect. (c) Stress–strain relations of above two defective graphene sheets.

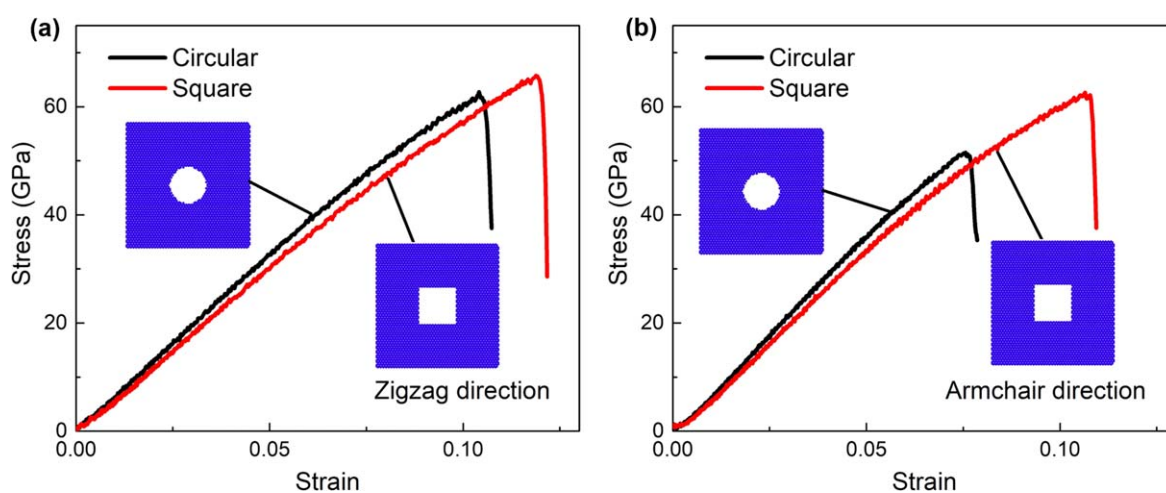


Figure 9. Stress–strain relations of graphene with a circular defect (diameter = $0.15L$) and graphene with a square defect (side length = $0.15L$) in the (a) zigzag and (b) armchair directions.

feasibility of modifying and enhancing the defective graphene as it is. The mechanism of degradation recovery lies in a reduced change in curvature during deformation, which is further solidified by theoretical quantification and stress-field analysis. This theory can also predict and pinpoint the location of the initiation of the fracture—where the curvature changes most significantly during the deformation. In addition, the influence of an elliptical defect on the mechanical properties of a graphene sheet is systematically studied. Finally, the degradation recovery potential of defects of various sizes is examined, showing that the initial defect that can create the highest degree of geometric asymmetry has the best potential for degradation recovery. This research, which investigates the recovery from defect-induced mechanical degradation and the influence of elliptical defect on the in-plane mechanical properties of a graphene sheet, sheds light on the new possibility of fine-tuning mechanical properties via defect engineering. The potential of mechanical degradation recovery via defect enlargement for other 2D materials as well as the recovery of out-of-plane mechanical properties will be covered in future work.

Acknowledgments

The authors acknowledge support from the Extreme Science and Engineering Discovery Environment (XSEDE) at the Pittsburgh Supercomputing Center (PSC) through allocation TG-DMR180085, by the National Science Foundation under grant number ACI-1548562. Additionally, the authors acknowledge support from an NVIDIA GPU Seed Grant and the Savio computational cluster resource provided by the Berkeley Research Computing program.

ORCID iDs

Grace X Gu  <https://orcid.org/0000-0001-7118-3228>

References

- [1] Novoselov K S, Geim A K, Morozov S V, Jiang D, Zhang Y, Dubonos S V, Grigorieva I V and Firsov A A 2004 Electric field effect in atomically thin carbon films *Science* **306** 666–9
- [2] Berger C *et al* 2004 Ultrathin epitaxial graphite: 2D electron gas properties and a route toward graphene-based nanoelectronics *J. Phys. Chem. B* **108** 19912–6
- [3] Withers F, Dubois M and Savchenko A K 2010 Electron properties of fluorinated single-layer graphene transistors *Phys. Rev. B* **82** 073403
- [4] Liu M, Yin X, Ulin-Avila E, Geng B, Zentgraf T, Ju L, Wang F and Zhang X 2011 A graphene-based broadband optical modulator *Nature* **474** 64
- [5] Balandin A A, Ghosh S, Bao W, Calizo I, Teweldebrhan D, Miao F and Lau C N 2008 Superior thermal conductivity of single-layer graphene *Nano Lett.* **8** 902–7
- [6] Balandin A A 2011 Thermal properties of graphene and nanostructured carbon materials *Nat. Mater.* **10** 569
- [7] Lee C, Wei X, Kysar J W and Hone J 2008 Measurement of the elastic properties and intrinsic strength of monolayer graphene *Science* **321** 385–8
- [8] Zhang P *et al* 2014 Fracture toughness of graphene *Nat. Commun.* **5** 3782
- [9] Chen C-T, Martin-Martinez F J, Ling S, Qin Z and Buehler M J 2017 Nacre-inspired design of graphene oxide–polydopamine nanocomposites for enhanced mechanical properties and multi-functionalities *Nano Futures* **1** 011003
- [10] Chen C T and Gu G X 2019 Effect of constituent materials on composite performance: exploring design strategies via machine learning *Adv. Theor. Simul.* **2** 1900056
- [11] Zheng B and Gu G X 2019 Tuning graphene mechanical anisotropy via defect engineering *Carbon* **155** 697–705
- [12] Young R J, Kinloch I A, Gong L and Novoselov K S 2012 The mechanics of graphene nanocomposites: a review *Compos. Sci. Technol.* **72** 1459–76
- [13] Wan S, Peng J, Li Y, Hu H, Jiang L and Cheng Q 2015 Use of synergistic interactions to fabricate strong, tough, and conductive artificial nacre based on graphene oxide and chitosan *ACS Nano* **9** 9830–6
- [14] Xu Z *et al* 2016 Ultrastiff and strong graphene fibers via full-scale synergetic defect engineering *Adv. Mater.* **28** 6449–56
- [15] Papageorgiou D G, Kinloch I A and Young R J 2017 Mechanical properties of graphene and graphene-based nanocomposites *Prog. Mater. Sci.* **90** 75–127
- [16] Martin-Olmos C, Rasool H I, Weiller B H and Gimzewski J K 2013 Graphene MEMS: AFM probe performance improvement *ACS Nano* **7** 4164–70
- [17] Bunch J S, van der Zande A M, Verbridge S S, Frank I W, Tanenbaum D M, Parpia J M, Craighead H G and McEuen P L 2007 Electromechanical resonators from graphene sheets *Science* **315** 490–3
- [18] Zhu J, Childress A S, Karakaya M, Dandeliya S, Srivastava A, Lin Y, Rao A M and Podila R 2016 Defect-engineered graphene for high-energy- and high-power-density supercapacitor devices *Adv. Mater.* **28** 7185–92
- [19] Wang Y, Shi Z, Huang Y, Ma Y, Wang C, Chen M and Chen Y 2009 Supercapacitor devices based on graphene materials *J. Phys. Chem. C* **113** 13103–7
- [20] Kim K S, Zhao Y, Jang H, Lee S Y, Kim J M, Kim K S, Ahn J-H, Kim P, Choi J-Y and Hong B H 2009 Large-scale pattern growth of graphene films for stretchable transparent electrodes *Nature* **457** 706
- [21] Jang H, Park Y J, Chen X, Das T, Kim M-S and Ahn J-H 2016 Graphene-based flexible and stretchable electronics *Adv. Mater.* **28** 4184–202
- [22] Cao Q, Geng X, Wang H, Wang P, Liu A, Lan Y and Peng Q 2018 A review of current development of graphene mechanics *Crystals* **8** 357
- [23] Cao G 2014 Atomistic studies of mechanical properties of graphene *Polymers* **6** 2404–32
- [24] Wei Y and Yang R 2018 Nanomechanics of graphene *Nat. Sci. Rev.* **6** 324–48
- [25] Akinwande D *et al* 2017 A review on mechanics and mechanical properties of 2D materials—Graphene and beyond *Extreme Mech. Lett.* **13** 42–77
- [26] Bao W, Miao F, Chen Z, Zhang H, Jang W, Dames C and Lau C N 2009 Controlled ripple texturing of suspended graphene and ultrathin graphite membranes *Nat. Nanotechnol.* **4** 562–6
- [27] Tapasztó L, Dumitrică T, Kim S J, Nemes-Incze P, Hwang C and Biró L P 2012 Breakdown of continuum mechanics for nanometre-wavelength rippling of graphene *Nat. Phys.* **8** 739–42
- [28] Deng S and Berry V 2016 Wrinkled, rippled and crumpled graphene: an overview of formation mechanism, electronic properties, and applications *Mater. Today* **19** 197–212

- [29] Xu W, Qin Z, Chen C-T, Kwag H R, Ma Q, Sarkar A, Buehler M J and Gracias D H 2017 Ultrathin thermoresponsive self-folding 3D graphene *Sci. Adv.* **3** e1701084
- [30] Shen B, Li Y, Yi D, Zhai W, Wei X and Zheng W 2017 Strong flexible polymer/graphene composite films with 3D saw-tooth folding for enhanced and tunable electromagnetic shielding *Carbon* **113** 55–62
- [31] Patra N, Wang B and Král P 2009 Nanodroplet activated and guided folding of graphene nanostructures *Nano Lett.* **9** 3766–71
- [32] Green A A and Hersam M C 2009 Solution phase production of graphene with controlled thickness via density differentiation *Nano Lett.* **9** 4031–6
- [33] Yi M and Shen Z 2015 A review on mechanical exfoliation for the scalable production of graphene *J. Mater. Chem. A* **3** 11700–15
- [34] Chen Z, Ren W, Gao L, Liu B, Pei S and Cheng H-M 2011 Three-dimensional flexible and conductive interconnected graphene networks grown by chemical vapour deposition *Nat. Mater.* **10** 424
- [35] Mattevi C, Kim H and Chhowalla M 2011 A review of chemical vapour deposition of graphene on copper *J. Mater. Chem.* **21** 3324–34
- [36] Sagaliansov I Y, Radchenko T M, Prylutsky Y I, Tatarenko V A and Szroeder P 2017 Mutual influence of uniaxial tensile strain and point defect pattern on electronic states in graphene *Eur. Phys. J. B* **90** 112
- [37] Radchenko T M, Tatarenko V A, Lizunov V V, Molodkin V B, Golentus I E, Sahalianov I Y and Prylutsky Y I 2019 Defect-pattern-induced fingerprints in the electron density of states of strained graphene layers: diffraction and simulation methods *Phys. Status Solidi B* **256** 1800406
- [38] Sahalianov I Y, Radchenko T M, Tatarenko V A and Prylutsky Y I 2018 Magnetic field-, strain-, and disorder-induced responses in an energy spectrum of graphene *Ann. Phys.* **398** 80–93
- [39] Sahalianov I Y, Radchenko T M, Tatarenko V A, Cuniberti G and Prylutsky Y I 2019 Straintronics in graphene: extra large electronic band gap induced by tensile and shear strains *J. Appl. Phys.* **126** 054302
- [40] Wang M C, Yan C, Ma L, Hu N and Chen M W 2012 Effect of defects on fracture strength of graphene sheets *Comput. Mater. Sci.* **54** 236–9
- [41] Hao F, Fang D and Xu Z 2011 Mechanical and thermal transport properties of graphene with defects *Appl. Phys. Lett.* **99** 041901
- [42] Ansari R, Ajori S and Motevalli B 2012 Mechanical properties of defective single-layered graphene sheets via molecular dynamics simulation *Superlatt. Microstruct.* **51** 274–89
- [43] Eshkalak K E, Sadeghzadeh S and Jalaly M 2018 Mechanical properties of defective hybrid graphene-boron nitride nanosheets: a molecular dynamics study *Comput. Mater. Sci.* **149** 170–81
- [44] Zandiatahbar A, Lee G-H, An S J, Lee S, Mathew N, Terrones M, Hayashi T, Picu C R, Hone J and Koratkar N 2014 Effect of defects on the intrinsic strength and stiffness of graphene *Nat. Commun.* **5** 3186
- [45] Zhao H, Min K and Aluru N R 2009 Size and chirality dependent elastic properties of graphene nanoribbons under uniaxial tension *Nano Lett.* **9** 3012–5
- [46] Plimpton S 1995 Fast parallel algorithms for short-range molecular dynamics *J. Comput. Phys.* **117** 1–19
- [47] Stuart S J, Tutein A B and Harrison J A 2000 A reactive potential for hydrocarbons with intermolecular interactions *J. Chem. Phys.* **112** 6472–86
- [48] Wei Y, Wu J, Yin H, Shi X, Yang R and Dresselhaus M 2012 The nature of strength enhancement and weakening by pentagon–heptagon defects in graphene *Nat. Mater.* **11** 759
- [49] Grantab R, Shenoy V B and Ruoff R S 2010 Anomalous strength characteristics of tilt grain boundaries in graphene *Science* **330** 946–8
- [50] Wang C, Liu Y, Lan L and Tan H 2013 Graphene wrinkling: formation, evolution and collapse *Nanoscale* **5** 4454–61
- [51] Zhang T, Li X, Kadkhodaei S and Gao H 2012 Flaw insensitive fracture in nanocrystalline graphene *Nano Lett.* **12** 4605–10
- [52] Hoover W G 1985 Canonical dynamics: equilibrium phase-space distributions *Phys. Rev. A* **31** 1695–7
- [53] Yazyev O V and Louie S G 2010 Topological defects in graphene: dislocations and grain boundaries *Phys. Rev. B* **81** 195420
- [54] Wehling T O, Yuan S, Lichtenstein A I, Geim A K and Katsnelson M I 2010 Resonant scattering by realistic impurities in graphene *Phys. Rev. Lett.* **105** 056802
- [55] Zhang H, Lee G and Cho K 2011 Thermal transport in graphene and effects of vacancy defects *Phys. Rev. B* **84** 115460